The impact of coastal phytoplankton blooms on ocean-atmosphere thermal energy exchange: Evidence from a two-way coupled numerical modeling system: PHYTOPLANKTON IMPACT ON AIR-SEA C...

7 authors, including:

Jason Keith Jolliff
United States Naval Research Laboratory
65 PUBLICATIONS   **1,039** CITATIONS

Travis A. Smith
United States Naval Research Laboratory
35 PUBLICATIONS   **217** CITATIONS

Robert Arnone
University of Southern Mississippi
277 PUBLICATIONS   **6,303** CITATIONS

Some of the authors of this publication are also working on these related projects:

Project   VIIRS val/cal View project

Project   Dynamic anomaly bio-physical hotspots in Gulf of MExico View project

The impact of coastal phytoplankton blooms on ocean-atmosphere thermal energy exchange: Evidence from a two-way coupled numerical modeling system

Jason K. Jolliff,[1] Travis A. Smith,[1] Charlie N. Barron,[1] Sergio deRada,[1] Stephanie C. Anderson,[1] Richard W. Gould,[1] and Robert A. Arnone[2]

[1] A set of sensitivity experiments are performed with a two-way coupled and nested ocean-atmosphere forecasting system in order to deconvolve how dense phytoplankton stocks in a coastal embayment may impact thermal energy exchange processes. Monterey Bay simulations parameterizing solar shortwave transparency in the surface ocean as an invariant oligotrophic oceanic water type estimate consistently colder sea surface temperature (SST) than simulations utilizing more realistic, spatially varying shortwave attenuation terms based on satellite estimates of surface algal pigment concentration. These SST differences lead to an ~88% increase in the cumulative turbulent thermal energy transfer from the ocean to the atmosphere over the three month simulation period. The result is a warmer simulated atmospheric boundary layer with respective local air temperature differences approaching ~2°C. This study suggests that the retention of shortwave solar flux by ocean flora may directly impact even short-term forecasts of coastal meteorological variables. **Citation:** Jolliff, J. K., T. A. Smith, C. N. Barron, S. deRada, S. C. Anderson, R. W. Gould, and R. A. Arnone (2012), The impact of coastal phytoplankton blooms on ocean-atmosphere thermal energy exchange: Evidence from a two-way coupled numerical modeling system, *Geophys. Res. Lett.*, *39*, L24607, doi:10.1029/2012GL053634.

1. Introduction

[2] Solar irradiance is the principal source of heat for the surface ocean. After transmission through the intervening atmosphere and reflection at the sea surface, the penetration of the remaining solar irradiance is dependent upon the absorption and scattering properties of both seawater and the dissolved and suspended particulate materials therein. The bulk shortwave solar irradiant intensity encompasses a broad spectral range (~280 to 2500 nm). Absorption of this energy at infrared and longer wavelengths (>700 nm) tends to be dominated by pure water [*Morel and Antoine*, 1994; *Smith and Baker*, 1981]. However towards the blue end of the

ocean spectral transparency window, phytoplankton pigments harvest the penetrative photon flux for photosynthesis. Biophysical rate limitations render this harvest remarkably inefficient; most of the energy is dissipated as heat. Hence the direct consequence of a variable surface ocean phytoplankton biomass is the corresponding modulation of Z_{hl}, the effective depth over which 95% of the in-water penetrative solar flux is absorbed [*Morel and Antoine*, 1994]. Indeed, global empirical relationships between surface chlorophyll-*a* concentration and Z_{hl} may be derived [see *Morel et al.*, 2007]. Subsumed in this simplified scenario are the associated and presumptively co-varying phytoplankton degradation materials that also absorb light significantly in the ultraviolet and shorter visible wavelengths [e.g., *Carder et al.*, 1989].

[3] The confounding factors of surface ocean heat losses, three-dimensional advection and diffusion, and variable solar forcing have prompted investigators to use numerical ocean circulation models to investigate the manifest ramifications of the "ocean biological feedback" (OBF) effect outlined above. These experiments have demonstrated non-negligible simulated SST sensitivity to the surface ocean's bio-optical variability [e.g., *Anderson et al.*, 2007; *Cahill et al.*, 2008; *Oschlies*, 2004; *Wu et al.*, 2007]. SST, in turn, is known to be a key variable that determines the magnitude and variability of turbulent air-sea transfers of heat; these exchange processes then further modulate SST. What remains largely unresolved is an understanding of how OBF may be modulating the fully coupled air-sea interaction and the time-dependent evolution of thermal variables in the upper ocean as well as the lower atmosphere.

2. Methods

[4] To begin to address the fundamental impact of OBF on thermal exchange processes at the interface of planetary boundary layers, a fully coupled ocean-atmosphere modeling system is required. To that end, we perform numerical experiments using the Coupled Ocean-Atmosphere Mesoscale Prediction System (COAMPS®, a registered trademark of the Naval Research Laboratory), a nested numerical modeling system developed at the Naval Research Laboratory (NRL) that allows for a two-way exchange of information between the atmospheric and oceanic numerical forecasting components. The COAMPS configuration for our Monterey Bay, California study region consists of two independent three-dimensional variational (3DVAR) atmosphere and ocean data assimilation systems and a coupler that functions as a router to distribute the model forecast fields between the oceanic and atmospheric forecast components. The atmospheric and oceanic model coupling occurs via the upper-

[1]Oceanography Division, Naval Research Laboratory, Stennis Space Center, Mississippi, USA.
[2]Department of Marine Science, University of Southern Mississippi, Stennis Space Center, Mississippi, USA.

Corresponding author: J. K. Jolliff, Oceanography Division, Naval Research Laboratory, Code 7331, Stennis Space Center, MS 39529, USA. (jason.jolliff@nrlssc.navy.mil)
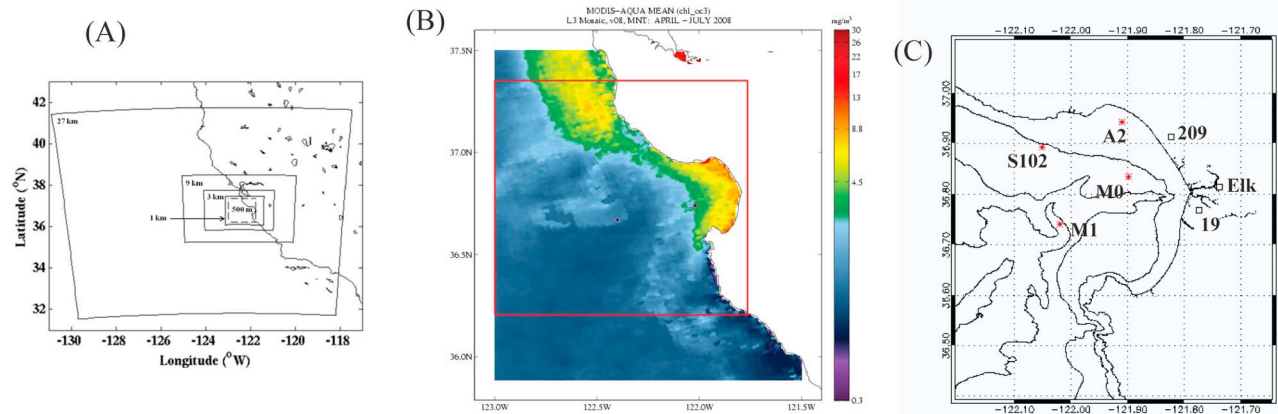
Figure 1. (a) COAMPS nested model configuration: outer atmospheric model nests begin at 27 km horizontal resolution and nest iteratively down to 9, 3, and 1 km. The inner ocean model nest, at 500 meter horizontal resolution and centered upon Monterey Bay, California, is indicated by the dashed line. (b) Composite MODIS image for the surface chlorophyll-*a* product; the inner nest ocean model domain is indicated by the red box. (c) Bathymetry map for Monterey Bay, California with reference locations as listed in Table 1 for Monterey Bay Aquarium Research Institute (MBARI) permanent moorings M1 and M0, and NRL temporary moorings S102 and A2 (red asterisks). Land locations for California Irrigation Management Information System (CIMIS) meteorological stations: (209) Watsonville West and (19) Castroville are indicated with a square. The Elkhorn Slough (Elk) reference site is approximate to the National Estuarine Research Reserve System (NERRS) weather station.

most oceanic model grid cell temperature and the lowest grid cell atmospheric model variables (temperature, humidity, wind velocity, pressure, and radiative fluxes). Bulk fluxes of heat energy exchange are calculated following the Coupled Ocean-Atmosphere Response, version 3 (COARE 3.0) scheme [*Fairall et al.*, 1996].

[5] The Navy Coastal Ocean Model (NCOM) [*Barron et al.*, 2006] serves as the ocean model component with assimilation performed via the Navy Coupled Ocean Data Assimilation (NCODA) 3DVAR system [*Cummings*, 2005]. The COAMPS domain configuration for Monterey Bay (Figure 1a) consists of a quadruple-nested atmospheric domain with 27, 9, 3, and 1 km horizontal spacing. The NCOM configuration consists of an inner nest with 500 meter horizontal grid spacing. It is initialized using fields interpolated from the global (1/8°) NCOM results [*Kara et al.*, 2006]; similar fields serve as boundary conditions during the 4-month simulation. This inner nest is executed in data-assimilative mode during a 1 month spin-up period (beginning on 1 April 2008) and then in non-data-assimilative mode (or 'free-run' mode) for the remaining three months of the simulation (ending 31 July 2008).

[6] Verification and validation of the COAMPS forecasting system may be found elsewhere [*Doyle et al.*, 2009; *Small et al.*, 2012]; here we focus on the modeling system's sensitivity to changes in the oceanic shortwave optical attenuation that arise as a result of surface ocean phytoplankton variability. Previous COAMPS applications in the Monterey Bay region have suggested that a 40% reduction factor for surface shortwave irradiance is warranted [*Shulman et al.*, 2007]. Such a reduction compensates for the inability of COAMPS to simulate the specific reflective effects of low-lying marine stratus clouds [*Doyle et al.*, 2009]. Here we present results from a 'reduced shortwave' series of numerical experiments.

[7] Specific to the simulated attenuation of solar shortwave in the ocean model, the default parameterization for COAMPS is the "Jerlov" [*Jerlov*, 1976] oceanic water Type IA implemented in a two-band shortwave extinction scheme popularized for physical ocean models by *Paulson and Simpson* [1977] (herein, 'PS77-IA'). The main feature to be distinguished here is that PS77-IA employs time/space invariant scalar quantities associated with an ideal oligotrophic state, thereby ignoring any potential optical variability in surface waters over the model domain. The PS77-1A parameterization is used for the control model simulation case (S1).

[8] An upgraded representation of shortwave attenuation is examined in the alternative simulation case (S2), which replaces the ideal oligotrophic conditions of PS77-IA with a satellite-based attenuation scheme that allows recent observations to guide attenuation levels. For this purpose, a 4-month composite is prepared based on sea surface chlorophyll (mg m^{-3}) estimates derived from the Moderate Resolution Imaging Spectroradiometer (MODIS) sensor and mapped to the inner ocean model nest (Figure 1b); each pixel in the composite product averages all clear observations of that pixel over the 4-month period. The two-dimensional surface chlorophyll fields are read into NCOM for calculations of the depth-dependent transmission of shortwave irradiance using the *Lee et al.* [2005] method. This scheme divides total solar shortwave into Photosynthetically Available Radiation (PAR; 350–700 nm) and longer (>700 nm) spectral components. The depth-dependent attenuation coefficient for the integrated PAR spectral range [$K_{PAR}(z)$] is then calculated based on the surface absorption and scattering coefficients. These optical coefficients are inferred from the satellite surface chlorophyll product using algorithms based on published 'Case I' relationships [*Morel*, 1988; *Morel et al.*, 2007]. A separate
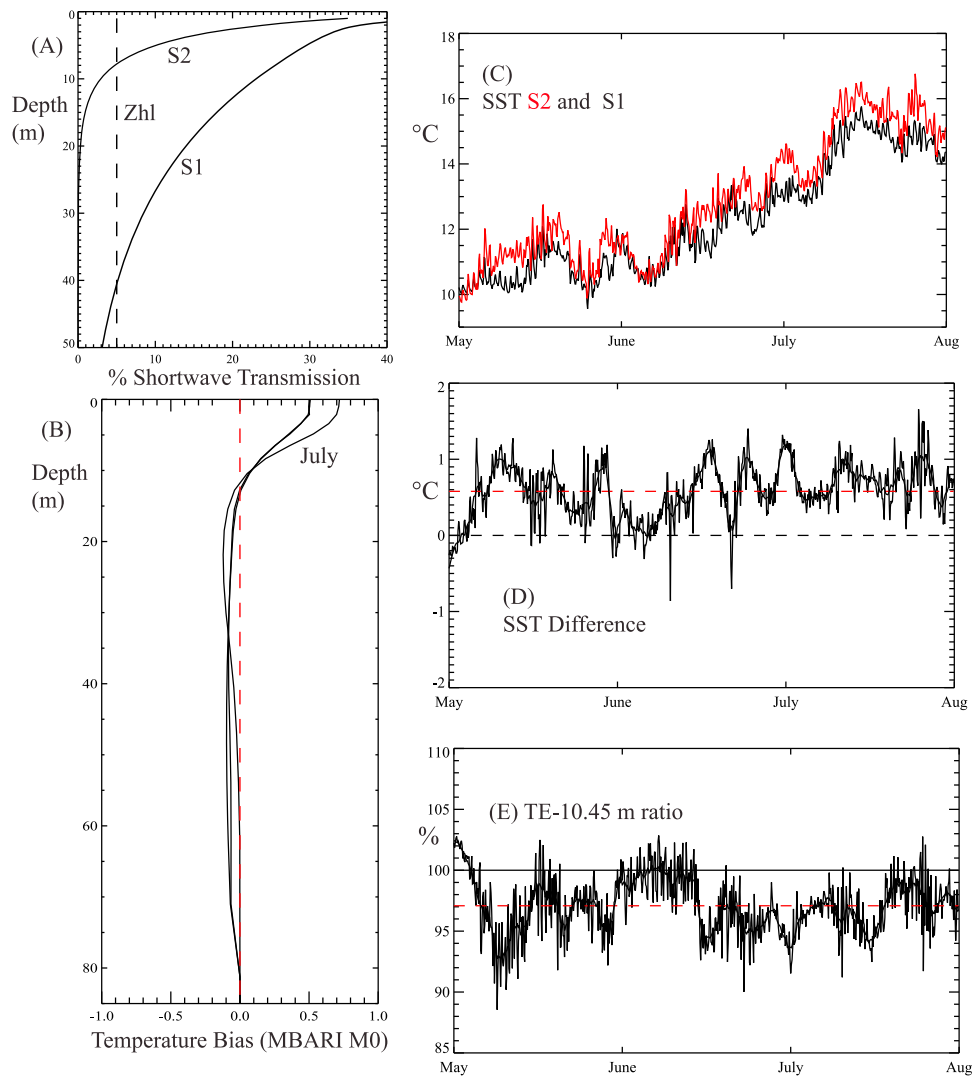
Figure 2. (a) Simulated shortwave radiation transmittance using the PS77-IA parameterization (S1) and the satellite-based method described in the text (S2) for the M0 reference location in Monterey Bay. (b) The temperature profile bias for each month at the M0 location is calculated by subtracting the mean monthly temperature profile of S1 from the mean profile of S2, the May and June profiles are nearly identical, the July profile is labeled. (c) The 3-hourly SST results for S2 (red) and S1 (black). (d) The 3-hourly SST difference (S2 - S1), the smoothed trend line (solid black) and the bias (dashed red) are shown. (e) The ratio of S1 depth-integrated thermal energy content (for the upper 10.45 meters) to the same as calculated for S2. As in Figure 2d, the smoothed series are shown as well as the respective biases (differences of the respective time series means; dashed red line).

analysis of in situ optical data [*Jolliff et al.*, 2012] confirmed these relationships to be reasonable for the Monterey Bay region.

[9] The nested modeling system domain is centered upon the Monterey Bay region of the U.S. West Coast (Figure 1a). Monterey Bay is a ∼40 km wide open embayment known for very high rates of biological productivity [*Wilkerson et al.*, 2000], particularly during the spring to summer upwelling season [*Chavez et al.*, 1991]. As is typical of eastern boundary upwelling systems, colder subsurface waters emerge at the surface along the coastal divergence, and rapid warming of these waters is concomitant with biological utilization of dissolved nutrients leading to persistent coastal eutrophication (defined here as >2.0 mg m^{-3} surface chlorophyll-*a*) [*Kudela and Dugdale*, 2000]. Simulated land/sea temperature comparison reference points are selected from the coupled model domain (Figure 1c) in order to assess the thermal impact of phytoplankton blooms inside Monterey Bay. These reference points correspond to temporary and permanent marine mooring locations and land surface meteorological observation stations.

3. Results

[10] In comparison to the satellite-based shortwave attenuation scheme, the PS77-IA parameterization overestimates Z_{hl} by 33 meters at mooring M0 (Figure 2a). The important distinction between the S1 and S2 attenuation profiles is that under the satellite-determined chlorophyll concentrations of S2, the upper decameter of the water column absorbs most of the penetrative shortwave. The result of this curtailed penetrative flux is evident in the temperature profile bias, i.e.,

Table 1. S1 and S2 Comparison Statistics[a]

S1 versus S2 for May-June-July	M1	M0	NRL - S102	NRL - A2
Latent Heat Flux Bias	3.79 W m^{-2}	4.7 W m^{-2}	3.9 W m^{-2}	3.46 W m^{-2}
Latent Heat Flux Amplitude, r^2	1.13,0.88	1.24,0.88	1.27,0.88	1.14,0.89
Total Latent Increase (%)	30.8	40.4	34.3	32.6
Turbulent Heat Flux Bias	4.33 W m^{-2}	5.22 W m^{-2}	4.11 W m^{-2}	3.9 W m^{-2}
Turbulent Heat Flux Amplitude, r^2	1.12,0.82	1.27,0.83	1.29,0.88	1.11,0.85
Total Turbulent Heat Flux Increase (%)	66.7	63.1	44.2	87.9
Air Temp. (2 m) Bias	0.39°C	0.51°C	0.60°C	0.39°C
Air Temp. (2 m) Amplitude, r^2	1.07,0.98	1.08,0.97	1.12,0.98	1.10,0.98
Maximum Air Temp. (2 m) Diff.	1.5°C	1.6°C	1.6°C	2.2°C
SST (1 m) Bias	0.45°C	0.57°C	0.64°C	0.43°C
SST (1 m) Amplitude, r^2	1.05,0.96	1.09,0.96	1.13,0.97	1.10,0.96
Maximum SST (1 m) Difference	1.55°C	1.70°C	1.77°C	1.60°C

[a]For each of the (4) marine reference points indicated in the top row, time series of simulated thermal variables (hourly results for May, June, and July) are extracted from each respective simulation (S1 and S2). Bias refers to the difference between the means calculated for each simulation time series: mean (S2 results) − mean(S1 results). Amplitude is the ratio of standard deviations: SD(S2)/SD(S1). The r^2 statistic is the square of the linear correlation coefficient between the two time series. The percentage increases (%) in the heat flux terms are calculated from the total thermal energy passing from the ocean to the atmosphere (F) during the respective three month free-run simulation periods for S1 and S2 following the formula: [F(S2) − F(S1)]/ F(S1) * 100. The turbulent heat flux is the sum of the latent and sensible heat fluxes.

the difference between the monthly average temperature profiles (Figure 2b). The July monthly bias is positive (S2 is warmer) by 0.7°C in the upper decamater; below this depth S2 is colder by ∼0.1–0.2°C. This comparative redistribution of thermal energy is to be expected based on the different shortwave attenuation profiles: neglecting advection and vertical mixing, the direct solar heating rate is inversely proportional to the heating layer thickness, Z_{hl}.

[11] The simulated temporal SST trends at reference mooring M0 are indicative of the spring transition from a well-mixed water column to increasing thermal stratification over the three months of the free-run simulation period (May–July; Figure 2c). SSTs in both simulations increase by at least ∼4°C over the transition period. Nonetheless, the three-month S2 warm bias is comparatively consistent at +0.57°C with the instantaneous SST difference ranging as high as ∼1.7°C (Figure 2d). The upper decameter integrated thermal energy in S1 fell as much as ∼10% lower than in S2 (Figure 2c) with a mean difference of 3%. The comparatively consistent SST bias over the free-run simulation period in conjunction with the high correlation of the S1 and S2 SST results ($r^2 = 0.96$) indicates that the main impact of the OBF effect in the S2 simulation is a change in the thermal exchange of energy between the simulated ocean and atmosphere.

[12] Indeed, the cumulative total turbulent thermal energy transfer (quantified as the sum of the latent and sensible heat flux to the atmosphere) increases by 87.9% at the model location corresponding to NRL temporary mooring A2 (Figure 1c and Table 1). Similarly, the corresponding increase for M0 is 63%. Wind speeds are largely the same in the two simulations, although some fine-scale local mismatches are evident (wind results not shown). This indicates that the increased thermal energy in the surface layer of S2 drives simulated differences in latent transfer via an increased SST and changes in the turbulent transfer coefficients of the *Fairall et al.* [1996] bulk flux scheme. Accordingly, the lower marine air temperatures at the mooring locations are elevated in the S2 simulation (Table 1). Both the SST and lower air temperature biases and maximum instantaneous differences closely match one another. The high correlation values (r^2) indicate that potential differences in advection (surface winds, currents) are not significantly impacting the simulation comparisons at fixed reference points inside Monterey Bay. The slight increase in

amplitude (the ratio of time series standard deviations) is indicative of a stronger diurnal warming signal in S2.

[13] The manifest result of the increased thermal energy transfer in S2 is an increase in the simulated air temperature for the marine atmospheric boundary layer (MABL) over Monterey Bay and adjacent coastal areas. Monthly air temperature profile biases prepared for the coastal land reference sites (Figure 1c) indicate a peak bias for July of +0.5°C at the Castroville meteorological reference station (Figure 3). All reference stations indicate the simulated temperature biases propagate to >400 m height. More detailed examination of the lower air temperature comparisons (Figure 3, bottom) reveal an enhanced diurnal warming signal that exceeds 1°C difference at the Castroville station on July 18. July daily maximum temperature differences are generally in the range of 0.5–1.0°C for the other land stations (data not shown).

[14] Hence over the course of the three month free-run simulations, the S2 version reveals an increasingly warm MABL over Monterey Bay (Figure 4). This warm perturbation is advected by the prevailing northwesterly winds towards the Salinas Valley (Figure 4c). The air temperature warming bias is concentrated inside Monterey Bay and is consistent with the MODIS chlorophyll composite imagery indicating phytoplankton blooms along the interior coastline of Monterey Bay (Figure 1b). In the July bias field (Figure 4c) an additional warm bias center is apparent outside of Monterey Bay along 36.8°N latitude. This appears to result from differences between the two simulations in the intensity of upwelling along the coast north of Monterey Bay. Further analysis of the ocean circulation changes are beyond the scope of this paper, but we note that they become increasingly evident as the free-run ocean model solution moves farther away in time from the constraints of the ocean data-assimilation period (April 2008).

4. Summary and Conclusions

[15] Here we show that simulated transfers of thermal energy between the ocean and atmosphere are significantly impacted by the enhanced optical attenuation attendant to coastal phytoplankton blooms. Mechanistically, the additional solar shortwave retained by surface phytoplankton stocks remains available to flux back into the lower atmosphere via turbulent heat flux losses, thereby resulting in a
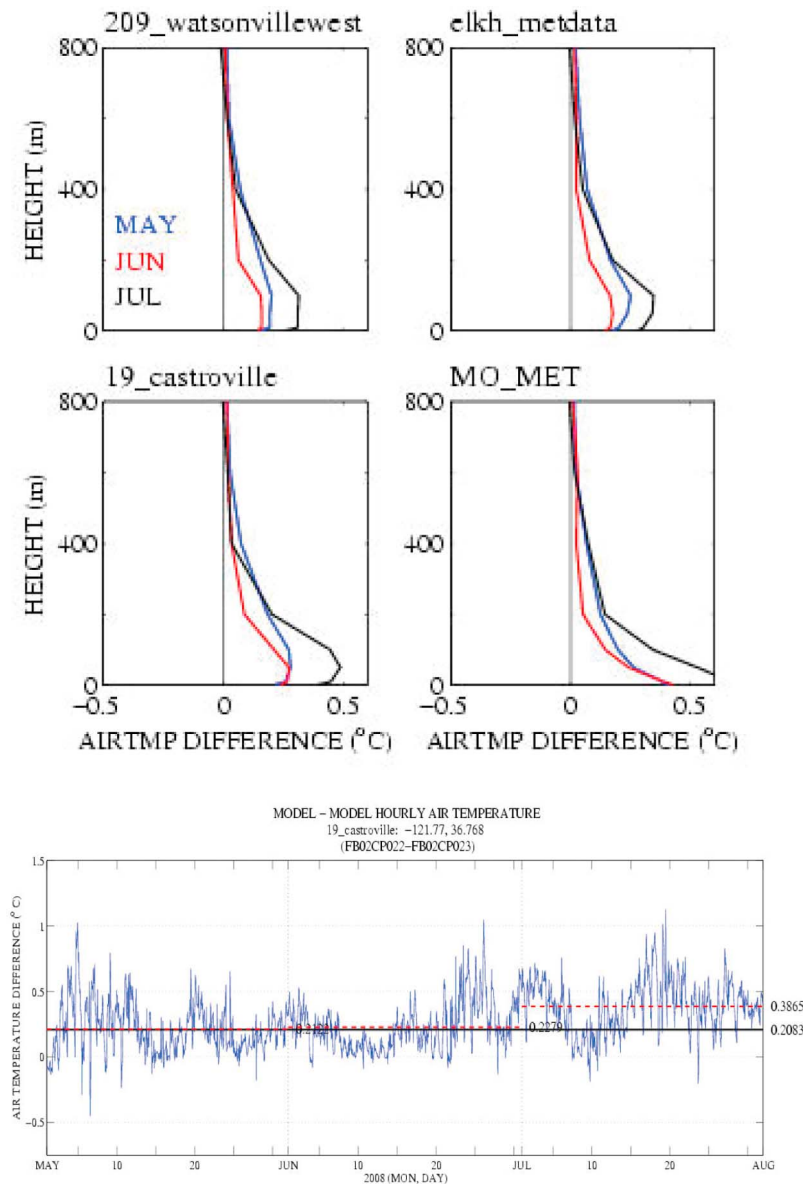
Figure 3. (top) For land locations, the mean air temperature profile from the atmospheric model simulation (S2) is subtracted from the same for S1. Positive values indicate a warming bias for S2. The reference station locations correspond to those mapped in Figure 1c. (bottom) The hourly lower air temperature difference (S2 − S1) is shown for reference land location 19 (CIMIS, Castroville). The 3-month time series bias is the solid black line, the monthly biases (May, June, and July) are indicated by the dashed red line.

comparative surplus of thermal energy in the MABL—energy that would otherwise be sequestered in the ocean. This 'reflux' of thermal energy then appears to have a significant impact on simulated lower air temperatures: up to ~1°C locally over land and ~2°C over water. These thermal atmospheric perturbations are similar to those obtained by *Shell et al.* [2003] using a coarse resolution coupled atmosphere-ocean general circulation model; however, here we show that this impact is pertinent to local scale air-sea fluxes on much shorter timescales.

[16] Accordingly, increasingly capable representations of optical attenuation due to dissolved and particulate seawater constituents appear justified for improving the potential accuracy of coupled ocean-atmosphere forecasting systems. In our numerical experiments, the surface chlorophyll-*a*

satellite product is used to estimate the in situ absorption coefficients required for our shortwave attenuation computations. This approach is reasonable for the Monterey Bay region since the measured surface water total absorption coefficients in the visible spectral range and the surface pigment concentrations are highly correlated in this system [*Jolliff et al.*, 2012]. For many other coastal environments, however, the additional optical property contributions from non-living organic matter as well as suspended sediments may also need to be considered explicitly and independently of the surface phytoplankton pigment distribution. More broadly applicable coastal numerical modeling efforts should account for these additional optical complexities.

[17] Our model results nonetheless leave open the question of how anthropogenic coastal eutrophication may also
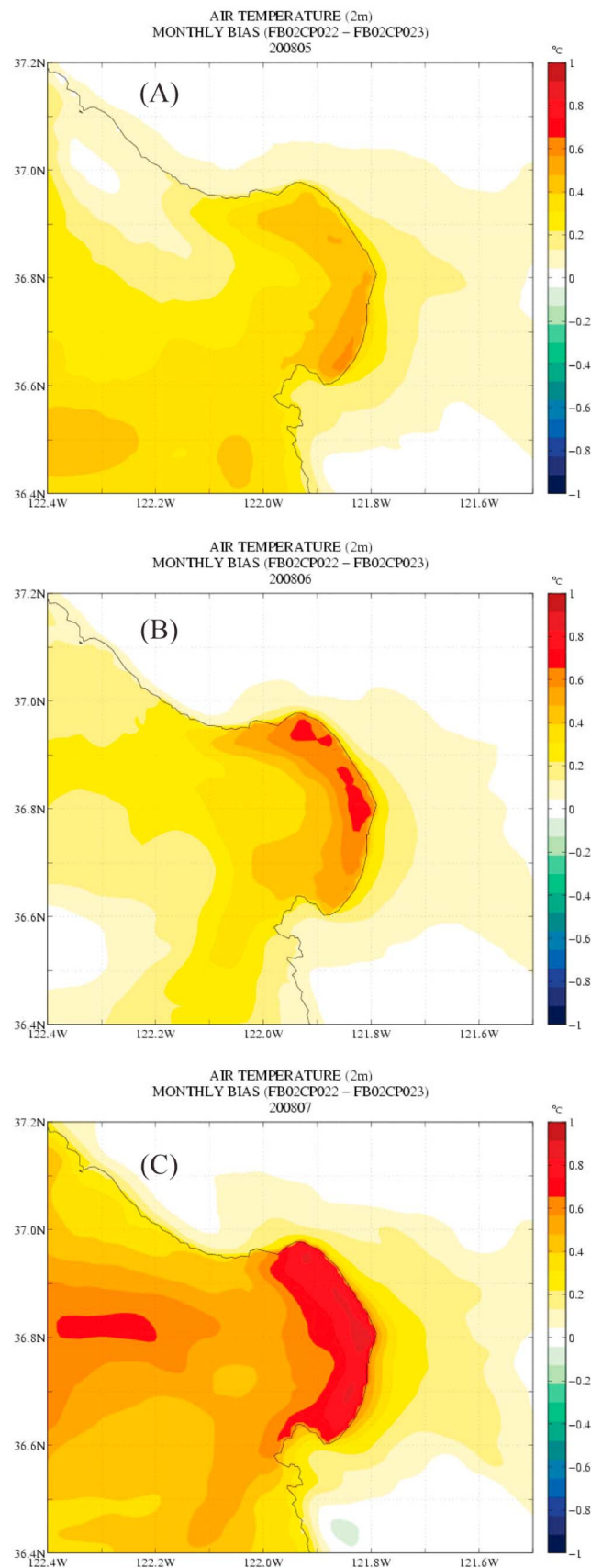
Figure 4. The spatial distribution of the respective lower air temperature (2 meter) biases [mean (S2) − mean(S1)] are shown for (A) May, (B) June, and (C) July of the simulations.

impact temperatures at the air-sea interface. The degree of thermal impact must be gauged with respect to a control point, which in our numerical experiments is the PS77-IA two-band abbreviation of the *Jerlov* [1976] Type IA oceanic surface water. Our calculations suggest that the PS77-IA attenuation scheme corresponds to approximately 0.13 mg m^{-3} surface chlorophyll, i.e., oligotrophic marine conditions. Given such clear natural waters as a control point, a significant increase in the surface absorption coefficients due to phytoplankton blooms, significant accumulation or discharge of colored dissolved organic matter (CDOM), or both events simultaneously may influence thermal variables at the air-sea interface. The effect may be significant enough to discernibly impact daily land surface temperature readings near the coast in the ~0.5–1.0°C range.

[19] The Editor thanks an anonymous reviewer for his/her assistance in evaluating this paper.

References

Anderson, W. G., A. Gnanadesikan, R. Hallberg, J. Dunne, and B. Samuels (2007), Impact of ocean color on the maintenance of the Pacific Cold Tongue, *Geophys. Res. Lett.*, *34*, L11609, doi:10.1029/2007GL030100.

Barron, C. N., A. B. Kara, P. J. Martin, R. C. Rhodes, and L. F. Smedstad (2006), Formulation, implementation and examination of vertical coordinate choices in the global Navy Coastal Ocean Model (NCOM), *Ocean Modell.*, *11*(3–4), 347–375, doi:10.1016/j.ocemod.2005.01.004.

Cahill, B., O. Schofield, R. Chant, J. Wilkin, E. Hunter, S. Glenn, and P. Bissett (2008), Dynamics of turbid buoyant plumes and the feedbacks on near-shore biogeochemistry and physics, *Geophys. Res. Lett.*, *35*, L10605, doi:10.1029/2008GL033595.

Carder, K. L., R. G. Steward, G. R. Harvey, and P. B. Ortner (1989), Marine humic and fulvic acids: Their effects on remote sensing of ocean chlorophyll, *Limnol. Oceanogr.*, *34*(1), 68–81, doi:10.4319/lo.1989.34.1.0068.

Chavez, F. P., R. T. Barber, A. Huyer, P. M. Kosro, S. R. Ramp, T. Stanton, and B. Rojas de Mendoila (1991), Horizontal advection and the distribution of nutrients in the coastal transition zone off Northern California: Effects on primary production, phytoplankton biomass and species composition, *J. Geophys. Res.*, *96*, 14,833–14,848, doi:10.1029/91JC01163.

Cummings, J. A. (2005), Operational multivariate ocean data assimilation, *Q. J. R. Meteorol. Soc.*, *131*, 3583–3604, doi:10.1256/qj.05.105.

Doyle, J. D., Q. Jiang, Y. Chao, and J. Farrara (2009), High-resolution real-time modeling of the marine atmospheric boundary layer in support of the AOSN-II field campaign, *Deep Sea Res., Part II*, *56*(3–5), 87–99, doi:10.1016/j.dsr2.2008.08.009.

Fairall, C. W., E. F. Bradley, D. P. Rogers, J. B. Edson, and G. S. Young (1996), Bulk parameterization of air-sea fluxes for TOGA COARE, *J. Geophys. Res.*, *101*, 3747–3764, doi:10.1029/95JC03205.

Jerlov, N. G. (1976), *Marine Optics*, 231 pp., Elsevier Sci., Amsterdam.

Jolliff, J. K., R. W. Gould Jr., B. Penta, W. J. Teague, S. DeRada, F. P. Chavez, and R. A. Arnone (2012), Water mass bio-optical properties in the Monterey Bay region: Fluorescence-based inference of shifts in phytoplankton photophysiology, *J. Geophys. Res.*, *117*, C07019, doi:10.1029/2011JC007568.

Kara, A. B., C. N. Barron, P. J. Martin, L. F. Smedstad, and R. C. Rhodes (2006), Validation of interannual simulations from the 1/8° global Navy Coastal Ocean Model (NCOM), *Ocean Modell.*, *11*, 376–398, doi:10.1016/j.ocemod.2005.01.003.

Kudela, R. M., and R. C. Dugdale (2000), Nutient regulation of phytoplankton productivity in Monterey Bay, California, *Deep Sea Res., Part II*, *47*, 1023–1053, doi:10.1016/S0967-0645(99)00135-6.

Lee, Z., K. Du, R. A. Arnone, S. Liew, and B. Penta (2005), Penetration of solar radiation in the upper ocean: A numerical model for oceanic and coastal waters, *J. Geophys. Res.*, *110*, C09019, doi:10.1029/2004JC002780.

Morel, A. (1988), Optical modeling of the upper ocean in relation to its biogenous matter content (case I waters), *J. Geophys. Res.*, *93*(C9), 10,749–10,768, doi:10.1029/JC093iC09p10749.

Morel, A., and D. Antoine (1994), Heating rate within the upper ocean in relation to its bio-optical state, *J. Phys. Oceanogr.*, *24*, 1652–1665, doi:10.1175/1520-0485(1994)024<1652:HRWTUO>2.0.CO;2.

Morel, A., Y. Huot, B. Gentili, P. J. Werdell, S. B. Hooker, and B. A. Franz (2007), Examining the consistency of products derived from various ocean color sensors in open ocean (Case 1) waters in the perspective of a multi-sensor approach, *Remote Sens. Environ.*, *111*(1), 69–88, doi:10.1016/j.rse.2007.03.012.

Oschlies, A. (2004), Feedbacks of biotically induced radiative heating on upper-ocean heat budget, circulation, and biological production in a coupled ecosystem-circulation model, *J. Geophys. Res.*, *109*, C12031, doi:10.1029/2004JC002430.

Paulson, C. A., and J. J. Simpson (1977), Irradiance measurements in the upper ocean, *J. Phys. Oceanogr.*, *7*, 952–956, doi:10.1175/1520-0485 (1977)007<0952:IMITUO>2.0.CO;2.

Shell, K. M., R. Frouin, S. Nakamoto, and R. C. J. Somerville (2003), Atmospheric response to solar radiation absorbed by phytoplankton, *J. Geophys. Res.*, *108*(D15), 4445, doi:10.1029/2003JD003440.

Shulman, I., J. Kindle, P. Martin, S. deRada, J. Doyle, B. Penta, S. Anderson, F. Chavez, J. Paduan, and S. Ramp (2007), Modeling of upwelling/ relaxation events with the Navy Coastal Ocean Model, *J. Geophys. Res.*, *112*, C06023, doi:10.1029/2006JC003946.

Small, R. J., S. Carniel, T. Campbell, J. Teixeira, and R. Allard (2012), The response of the Ligurian and Tyrrhenian Seas to a summer Mistral event: A coupled atmosphere–ocean approach, *Ocean Modell.*, *48*(0), 30–44, doi:10.1016/j.ocemod.2012.02.003.

Smith, R. C., and K. S. Baker (1981), Optical properties of the clearest natural waters (200–800 nm), *Appl. Opt.*, *20*(2), 177–184, doi:10.1364/ AO.20.000177.

Wilkerson, F. P., R. C. Dugdale, R. M. Kudela, and F. P. Chavez (2000), Biomass and productivity in Monterey Bay, California: Contribution of the large phytoplankton, *Deep Sea Res., Part II*, *47*(5–6), 1003–1022, doi:10.1016/S0967-0645(99)00134-4.

Wu, Y., C. C. L. Tang, S. Sathyendranath, and T. Platt (2007), The impact of bio-optical heating on the properties of the upper ocean: A sensitivity study using a 3-D circulation model for the Labrador Sea, *Deep Sea Res., Part II*, *54*, 2630–2642, doi:10.1016/j.dsr2.2007.08.019.